

The role of extended corona in formation of emission lines and continuum in AGN

A. Kurpiewski¹, J. Kuraszkiewicz², and B. Czerny²

¹*Astronomical Observatory of Warsaw University, Aleje Ujazdowskie 4, 00-478 Warsaw, Poland*

²*N. Copernicus Astronomical Centre, Bartycka 18, 00-716 Warsaw, Poland*

5 March 2018

ABSTRACT

We study a model of an accretion disc surrounded by an extended corona of the temperature $10^7 - 10^8$ K. This corona modifies the disk spectrum since it redirects a significant fraction of the emission from the central parts towards the more distant parts of the disk. The same corona is indirectly the source of the broad emission lines because we expect the formation of cool clouds at the basis of the corona due to thermal instabilities. We model the number of the clouds and their motion through the corona adopting a few different physically sound assumptions.

Comparing the predicted optical/UV continua and emission line ratios and profiles with the observed values we favor a particular model of a typical quasar. It radiates at ~ 0.5 of the Eddington luminosity, the corona surrounding the disk is additionally heated in excess of the Inverse Compton heating, and the broad line clouds are most probably destroyed when accelerated vertically above the sound speed within the corona.

Key words: galaxies: active – quasars: emission lines, accretion, accretion discs – line: formation – line: profiles.

1 INTRODUCTION

There is a general agreement that the nuclear activity of galaxies (with exception of starburst galaxies) is powered by accretion of interstellar gas onto a massive black hole (e.g. Rees 1984). The accretion flow most probably forms a kind of disc structure due to an excess of angular momentum.

The evidence of such disc-like structure is observed directly in HST pictures of the galaxy M87 at a distance of several pc from the center (Harms et al. 1994) and even up to 0.009 pc in the case of the galaxy NGC 4258 due to the presence of a water maser (Greenhill et al. 1995). Closer in the accretion flow is clearly two-phase. The cold gas most probably forms a relatively flat configuration, either in a form of an accretion disc or blobs. This material is embedded in a hot medium.

There are several observational arguments in favour of this general scenario.

Disc-like geometry of the cold phase explains the lack of significant absorption in quasars and Seyfert 1 galaxies as well as the presence of the X-ray spectral features in Seyfert 1 galaxies due to reprocessing by cool optically thick gas (i.e. the reflection component) covering approximately half of the sky for the source of X-rays (e.g. Pounds et al 1990, Matsuoka et al. 1990; for a review, see Mushotzky, Done & Pounds 1993). Additional support for the disc-like geometry

and Keplerian motion comes from determination of the shape of the K_α line from ASCA data (Fabian et al. 1994). The reflection component is not seen in quasars (Williams et al. 1992) most probably due to higher ionization stage of the gas (e.g. Życki et al. 1994, Życki & Czerny 1994).

The hot optically thin medium is required to explain the generation of the observed hard X-ray emission extending up to a few hundreds of keV (see Mushotzky et al. 1993). It most probably forms a kind of corona above the cold layer of the gas although an alternative view was also suggested (X-ray emission coming from shocks formed by gas outflowing along the symmetry axis, e.g. Henri & Pelletier 1991).

The heating mechanism of the corona, its structure and radial extension are presently unknown.

In the innermost parts of the flow a (sometimes considerable) fraction of the total gravitational energy of accreting gas has to be dissipated in the hot corona to provide both the X-ray bolometric luminosity and the extension of the emitted spectrum into high frequencies. Most probable emission mechanism is the Compton upscattering of the photons emitted by the cool gas by hot thermal electrons. The medium is not necessarily uniform, as we observe both the effect of moderate Comptonization (modification of the high frequency tail of the big bump emission seen in soft X-ray band in a number of sources, e.g. Czerny & Elvis 1987,

Wilkes & Elvis 1987, Walter & Fink 1993) as well as significant (but still unsaturated) Comptonization which leads to formation of the hard X-ray power law. It suggests that hard X-ray emission is perhaps produced in hotter, maybe magnetically driven compact active regions (e.g. Haardt, Maraschi & Ghisellini 1994, Stern et al. 1995) embedded, or surrounded by still hot but cooler plasma. Stochastic nature of the X-ray variability supports this view (Czerny & Lehto 1996).

In the outer parts of the flow the amount of energy available is small and the radiation emitted there does not practically contribute to the bolometric luminosity of the source and these regions are even less understood than the innermost flow. On the other hand the formation of the Compton-heated corona seems to be inevitable if only the outer parts of the disc are not shielded from the radiation coming from innermost parts (e.g. Begelman, McKee and Shields 1983, Begelman & McKee 1983, Ostriker, McKee & Klein 1991 - hereafter OMK, Raymond 1993). The existence of such a corona is actually observed in X-ray binaries (e.g. White & Holt 1982, McClintock et al. 1982, Fabian & Guilbert 1982). The existence of such a corona in AGN may have very significant influence on the observed spectrum.

The principal role of the corona surrounding the disc-like flow at a radius $\sim 0.01 - 1$ pc is not in the direct dissipation of the energy but in redirecting the radiation generated in the inner parts towards outer parts of the disc by almost elastic scattering. The direct irradiation in the case of AGN is not efficient unless the source of radiation is situated high above the disc surface. The disc surface in AGN does not flare in its inner parts, according to the widely adopted description of the radiation pressure dominated disc by Shakura and Sunyaev (1973) and in its outer flaring parts does not cover more than a per cent of the sky of the central X-ray source (e.g. Hure et al. 1994, Siemiginowska, Czerny & Kostyunin 1996).

The irradiation of the disc surface due to the scattering by the corona has two consequences: (i) the irradiation modifies the optical/UV continuum emitted by the disc and (ii) it leads to line formation at the basis of the corona thus contributing significantly to the observed Broad Emission Lines. Both effects are the subject of our study, with the aim to confirm the presence of the outer corona and to constrain its properties.

The plan of this paper is following. The description of the model of the corona and the method of computation of the continuum emission of the disc and line intensities and profiles from clouds forming in the disk/boundary layer is described in Section 2. In Section 3 we present the results for a range of model parameters and compare them with observations as well as we discuss the consequences of the model. Conclusions are given in Section 4.

2 THE MODEL OF THE CONTINUUM AND LINE EMISSION

2.1 Structure of the corona and location of the source of photons

The model of the corona above the outer parts of an accretion disc ($0.01 - 1$ pc) is based on the theory of the two-phase

equilibrium studied originally by Spitzer (1978) and further developed in the context of AGN in a number of papers, starting from Krolik, McKee and Tarter (1981) (hereafter KMT).

The temperature of the corona is mainly constrained by the inverse Compton heating and cooling by the incident radiation. The corona is irradiated by three different radiation sources: the high-energy central UV/X-ray source, radiation from the central source that has been scattered in corona and lower energy radiation from underlying viscous accretion disc. The central hard X-ray emission and the central thermal emission (for the most part UV) of the disc are both represented as a point like source located at a height H_X along the symmetry axis. Although in reality both emission regions are extended most of the energy is released within a few gravitational radii from the black hole which is $\sim 10^{-4}$ or less of the outer radius of a corona so the extension of the central source can be neglected. In our calculations we take half of the total disk luminosity as the value of central thermal luminosity. The proportion of total X-ray luminosity to central thermal luminosity is discussed in Sec. 2.3.1.

Following KMT and OMK we denote the inverse Compton temperature of the direct radiation (i.e. from the central source) by T_{IC} . For the spectrum of quasars used by KMT the value of T_{IC} is $\sim 10^8$ K (KMT), but allowing for more emission from "big blue bump" reduces T_{IC} to $\sim 10^7$ K (Mathews & Ferland 1987, Fabian et al. 1986). The presence of additional heating besides inverse Compton process does not modify the basic picture (if the heating rate is proportional to the gas density, e.g. Yaqoob 1990). However, it can raise the temperature of the corona above the inverse Compton limit, thus decoupling its value from the shape of the incident radiation spectrum. Therefore, we can treat the maximum value of the surface temperature of the corona, T_C , as a free parameter of the model.

Including scattered and disc components of irradiation, as well as bremsstrahlung cooling process near base of the corona, the temperature of the corona (constant in the vertical direction) is (OMK)

$$T_{cor(r)} = \frac{T_C}{2} \frac{F_{dir(r)} + F_{scat(r)} + F_{visc(r)}(T_{visc(r)}/T_C)}{F}, \quad (1)$$

where

$$F(r) = F_{dir(r)} + F_{scat(r)} + F_{visc(r)} \quad (2)$$

is total radiative flux at the base of the corona from all sources of irradiation. Indices 'dir', 'scat' and 'visc' are related to direct, scattered and disc components respectively and T_{visc} is the temperature of radiation emitted locally from the disc (F_{visc}).

The fraction of the central direct radiation (F_{dir}) and radiation scattered by the corona (F_{scat}) towards the disc at a radius r is given by simple analytical formulae of OMK in the case of sources with low ratio of the luminosity to the Eddington luminosity.

If the luminosity of the source is closer to the Eddington luminosity the corona is optically thicker and multiple scatterings play a significant role. In this case the numerical computations are necessary but the results are given in the paper of Murray et al. (1994) - hereafter MCKM - for a few sets of model parameters.

We use both the papers of OMK and MCKM to calculate the direct and scattered radiative flux irradiated the disk at a given radius. Therefore we follow the assumptions about the corona structure and the geometry made in those papers.

The corona extends up to 0.2 of the true maximum radius where the thermal energy of the gas particle $\sim kT_C$ is balanced by gravitational energy of the particle $\frac{GM\mu}{r}$

$$r_C = \frac{GM\mu}{kT_C} \approx \frac{10^{10}}{T_{C8}} \left(\frac{M}{M_\odot} \right) \text{cm}, \quad (3)$$

where T_{C8} is the maximum surface temperature of the corona expressed in units of 10^8 K, μ is the mean mass per particle ($\mu = 0.61m_p$ for fully ionized gas of cosmic abundances) and M is the mass of the black hole.

The ionization parameter Ξ (KMT) at the basis of the corona is equal (McKee & Begelman 1990)

$$\Xi_{b(r)} \approx 1.3T_{cor8(r)}^{-3/2}, \quad (4)$$

assuming that at higher densities bremsstrahlung is the only atomic cooling process. Since the ionization parameter is defined as a ratio of the incident radiation pressure to the gas pressure, its value determines the density at the basis of the corona (see Section 2.3.2).

2.2 Computation of the optical/UV continuum

2.2.1 Heating by viscous dissipation

Accretion disc is heated by dissipation of the gravitational energy of the gas through viscous forces. The radiative flux which corresponds with this energy for the disc with nonrotating black hole is given by (Page & Thorne 1974)

$$F_{visc(r)} = \frac{3GM\dot{M}}{8\pi r_g^3} \cdot f(r) \quad (5)$$

$$f(r) = \frac{\left[\sqrt{r} - \sqrt{3} + \sqrt{\frac{3}{8}} \ln \left(\frac{2-\sqrt{2}}{2+\sqrt{2}} \frac{\sqrt{r} + \sqrt{\frac{3}{2}}}{\sqrt{r} - \sqrt{\frac{3}{2}}} \right) \right]}{r^{\frac{5}{2}}(r - \frac{3}{2})}, \quad (6)$$

where

$$r_g = \frac{2GM}{c^2} \approx 3.01 \cdot 10^{-5} T_{C8} r_C \quad (7)$$

is the Schwarzschild radius, and

$$\dot{M} = \frac{L_{visc}}{\varepsilon c^2} \quad (8)$$

is the accretion rate. The efficiency ε is $\sim 5.6\%$ for a non-rotating black hole. In equations (5) and (6) the radius r is expressed in r_g units.

This picture does not leave any room for the X-ray emission. Actually, a fraction of energy due to accretion is dissipated in the form of X-rays. However, reliable predictions of that fraction as a function of radius are not available (see e.g. Witt et al. 1996). On the other hand the efficiency of accretion is most probably higher than adopted as the black hole may well be rotating, increasing the bolometric luminosity easily by a factor few. Therefore we describe the accretion disc emission as above but we allow that the total luminosity of the central source L may be higher than the disc luminosity L_{visc} due to the contribution from unaccounted X-ray emission.

2.2.2 Direct radiative heating of the disc

The additional radiation flux heating the disc is the flux of radiation from the central UV/X-ray source with luminosity L

$$F_{dir(r)} = (1 - A) \frac{L}{4\pi(r^2 + H_X^2)} f_{dir(r)} \cos \theta_{dir(r)} \quad (9)$$

where A is the albedo of the disc, $\theta_{dir(r)}$ is the angle between the incident ray and the normal to the disc at r , and

$$f = \frac{F}{L/4\pi r^2} \quad (10)$$

is used by OMK and MCKM dimensionless factor, which is the ratio of the radiation flux at the base of the corona to the unattenuated flux from the central source (in this definition in the denominator the component H_X^2 is neglected). To determine the factor f_{dir} we use the results of OMK or MCKM papers as we mentioned in Sec. 2.1. We assume $A=0.5$ as an appropriate value for quasars because the disc surface is partially ionized (see e.g. Życki et al. 1994).

2.2.3 Heating by corona

To describe the effect of irradiation by photons from the central source scattered towards the disc surface by extended corona we also use the method described in Sec. 2.1 to determine the scattered radiation flux

$$F_{scat(r)} = (1 - A) \frac{L}{4\pi r^2} f_{scat(r)} \langle \cos \theta_{scat} \rangle, \quad (11)$$

where $\langle \theta_{scat} \rangle$ is the angle between the direction from the scattering point and the normal to the disc at r , averaged over the whole volume of the corona. We determine the factor $f_{scat(r)} \langle \cos \theta_{scat} \rangle$ from OMK or MCKM papers. We adopt the same albedo as for the direct flux.

2.2.4 Computation of the spectrum

The effective temperature of the disc photosphere is given by

$$T_{eff(r)} = \left(\frac{F_{visc(r)} + F_{dir(r)} + F_{scat(r)}}{\sigma} \right)^{\frac{1}{4}}. \quad (12)$$

Assuming the black body emission from the disc, one can calculate the shape of continuum as follows

$$f_\nu = 2\pi \int_{3r_g}^{r_{max}} r B_\nu [T_{eff(r)}] dr, \quad (13)$$

where B_ν is the Planck function and r_{max} is the outer radius of the disc (in calculations we assume $r_{max} = r_C$).

We neglect the modification of the disc spectrum due to electron scattering. Although such effects were discussed by a number of authors (e.g. Czerny & Elvis 1987, Ross & Fabian 1993, Shimura & Takahara 1995) these corrections strongly depend on the accuracy of the description of atomic processes as well as assumptions on the disc viscosity.

2.3 The spectrum of the central source and the emission lines

2.3.1 Incident radiation spectrum

The computations of the continuum given in Sect. 2.2 cover only the optical/UV band as only the knowledge of the total X-ray luminosity, but not the shape of the primary X-ray emission, was required to compute the thermal emission of the disc dominating in this spectral band. On the other hand the computations of the strength of the emission lines require the determination of the spectrum in the EUV and X-ray band as well.

Therefore, for the purpose of calculating emission lines we use the spectral shapes which approximate well the observed overall spectra of Seyfert galaxies and quasars.

The shape of the big blue bump is parametrized in a similar way as by Mathews & Ferland (1987). However, we adjusted parametrization in agreement with the present observational data and we adopted interpolation to give the ratio of the bolometric luminosities of the big blue bump to X-rays equal ~ 1 for Seyfert galaxies and ~ 10 for quasars. The details of this parametrization are given in Appendix. The inverse Compton temperatures for these two spectra are $5.8 \cdot 10^7$ K for Seyfert galaxies and $1.1 \cdot 10^7$ K for quasars.

2.3.2 Local line emissivity

We assume that the high ionization emission lines come from the clouds which form in the narrow intermediate zone between an accretion disc and a hot corona. Thermal instability of irradiated gas at intermediate temperatures causes discontinuous transition between a disc and a corona (Begelman, McKee & Shields 1983), if only radiative processes are taken into account. In realistic situation, when some level of a turbulence is present in the medium, we may expect the spontaneous formation of the cool clumps embedded in the hot coronal plasma in a relatively narrow transitory zone (Różańska & Czerny 1996).

The column density of the clouds is not determined precisely but the estimates based of the relative efficiency of conduction and thermal processes give values of the same order as values expected for the clouds forming the Broad Line Region. Therefore we assume for all the clouds the column density equal 10^{23} cm^{-2} .

Cloud parameters (density n_{cl} and temperature T_{cl}) at a given radius are determined by two requirements. This first condition is the pressure equilibrium with the hot medium at the basis of the corona. The second condition, in the case of optically very thin plasma, should be the settlement on the lower stable branch at the $\Xi - T$ curve (KMT). However, this branch is not applicable for media of higher optical depth. Since we do not expect clouds to cool below the local effective temperature of the disk surface, we assume their temperature to be at that value, $T_{cl} = T_{eff}$. Therefore we adopt the condition

$$n_{cl(r)} = n_{d(r)} = n_{b(r)} \frac{T_{cor(r)}}{T_{eff(r)}} = n_{b(r)} \frac{T_{cor(r)}}{T_{cl(r)}} \quad (14)$$

where $n_{b(r)}$ is the density at the basis of the corona determined from the value of the ionization parameter Ξ_b and $T_{cor(r)}$ and $T_{eff(r)}$ are given by eq. (1) and (12).

We discuss the kinematics of the clouds in Sect. 2.3.3 since it is essential for computation of the line profiles. However, cloud motion influences the line intensities as well.

Since the clouds are blown out radiatively from the formation region they do not form a flat layer on the top of a disc but they are fully exposed to the incident radiation flux so the inclination angle of the direct incident flux does not have to be included through the cosine factor, as it is the case for the disk surface.

We calculate the emissivity of several emission lines (see Table 5 for the list) using the photoionization code CLOUDY. The calculations are made for a grid of radii resulting from the used range of n_{cl} : $10^9 - 10^{13} \text{ cm}^{-3}$ (the same for all models). For each radius separately we calculate the contribution to emission lines assuming the local value of the total heating flux $F(r)$ given by eq. (2),(5),(6),(9),(11), density $n_{d(r)}$ from eq. (14) and fixing the column density $N_H = 10^{23} \text{ cm}^{-2}$.

2.3.3 Radial dependence of number of clouds

Clouds forming in the transition layer between the disk and the corona does not necessarily cover the disk surface uniformly. Local number of clouds give weight to the local emissivity thus influencing both the line ratios and line profiles. The number of clouds, $N_{(r)}$, existing at a given radius depends both on the cloud formation rate, $\dot{N}_{(r)}$, and expected life time of a cloud, $t_{(r)}$

$$N_{(r)} = \dot{N}_{(r)} t_{(r)}. \quad (15)$$

As the detailed process of cloud formation and destruction is not well understood we discuss a few representative cases based on available estimates.

We consider two cases of the cloud formation process. In the first case we assume that only one cloud can form at a given moment and a given radius and the formation time is given by the characteristic isobaric cooling time, $\tau_{(r)}$ (McKee & Begelman 1990)

$$\text{case(I)} \quad \dot{N}_{(r)} \sim \frac{1}{\tau_{(r)}} \sim n_{b(r)}. \quad (16)$$

In the second case we assume that the clouds form in the entire instability zone therefore the number of the clouds forming at the same time is related to ratio of the zone geometrical thickness ΔZ , which is of order of the Field length (e.g. Różańska & Czerny 1996) to the size of the cloud, $r_{cl(r)} = N_H / n_{cl(r)}$

$$\text{case(II)} \quad \dot{N}_{(r)} \sim \frac{\Delta Z_{(r)}}{r_{cl(r)} \tau_{(r)}} \sim n_{cl(r)}. \quad (17)$$

We describe the destruction process using three different approaches. In the case (i) we assume that the clouds survive only within the instability zone. As they move through the zone upwards under the influence of the radiation from the disk surface their life time is given by the travel time through the zone ΔZ . We assume that the radiation acceleration is constant. It gives us the relation

$$\text{case(i)} \quad t_{(r)} \sim \frac{1}{\sqrt{n_{b(r)}}}. \quad (18)$$

In the case (ii) we assume that clouds survive even outside the instability zone but undergo the destruction due to conduction, evaporating into surrounding hot corona. The timescale of such a process is given by McKee & Begelman (1990)

Table 1. The models of radial dependence of number of clouds.

Model	Cases from Sec. 2.3.3	The radial dependence
a	(I)(i)	$\sqrt{n_{b(r)}}$
b	(I)(ii)	const.
c	(I)(iii)	$n_{b(r)}$
d	(II)(i)	$\sqrt{n_{b(r)}/T_{cl(r)}}$
e	(II)(ii)	$T_{cl(r)}$
f	(II)(iii)	$n_{cl(r)}$

$$\text{case(ii)} \quad t_{(r)} \sim \frac{1}{n_{b(r)}}. \quad (19)$$

In the case (iii) we assume that clouds are accelerated so efficiently by the radiation pressure that they reach soon the velocities exceeding the local sound velocity in the corona. Reaching this terminal velocity of ~ 2000 km/s they are destroyed by dynamical instabilities. Since we assume that the radiation acceleration of the clouds is independent from the disk radius the time needed to reach this terminal velocity is also constant if small variations of the corona temperature with the radius are ignored. In that case

$$\text{case(iii)} \quad t_{(r)} = \text{const.} \quad (20)$$

We summarize the six models of the number of clouds $N_{(r)}$ in Table 1.

2.3.4 Line profiles

We assume that the velocity field of the emitting clouds consists of the Keplerian orbital motion and the outflow perpendicular to the disc surface.

In our computations of the orbital motion we follow the method of Chen and Halpern (1989), including the relativistic effects. Their procedure requires the specific intensity from the disc surface

$$I_{(r,\nu_e)} = \frac{1}{4\pi} \epsilon_{(r)} \cdot \frac{e^{-\frac{(\nu_e - \nu_0)^2}{2\sigma^2}}}{(2\pi)^{1/2}\sigma} [\text{erg ss}^{-1} \text{cm}^{-2} \text{sr}^{-1} \text{Hz}^{-1}] \quad (21)$$

where $\epsilon_{(r)}$ is the local emissivity of the clouds (see Sec. 2.3.2) and the exponential factor is related to local broadening of the emission line. The broadening (due to electron scattering or turbulence e.g.) is characterized by quantity σ , and ν_e , ν_0 are the emitted and rest frequencies. After Chen and Halpern (1989) we use in our calculations $\sigma/\nu_0 = 0.03$.

The vertical motion is computed assuming that the acceleration of the clouds is constant, i.e. the velocity increases linearly with the distance from the disc surface. Maximum velocity is constrained by the cloud destruction.

Since the line profiles are not strongly dependent on the detailed description of the vertical motion as the orbital velocity is usually much higher than the vertical one we do not distinguish between the three cases introduced in Section 2.3.3 and in all cases we assume that the clouds move under the influence of constant radiative acceleration and reach the same terminal velocity equal 2000 km/s, independently from the disk radius, as expected in case (iii).

3 RESULTS AND DISCUSSION

We calculate the local radiation flux at the disc surface for the following parameters

$$M = 10^8 M_\odot$$

$$\varepsilon = 0.056$$

$$T_C = 10^8 \text{ K}; 10^7 \text{ K}$$

$$L = 0.01L_E; 0.34L_E; 0.59L_E$$

$$H_X = 3.32r_g; 33.2r_g.$$

The second value of the height could only be used in the calculations of the low luminosity cases as the numerical solutions of the high luminosity corona structure (MCKM) are available only for the first value. In agreement with generally accepted trend that low ratios of luminosity to the Eddington luminosity are appropriate for Seyfert galaxies and luminosities closer to the Eddington limit are appropriate for quasars, we use Seyfert galaxies spectrum for $L = 0.01L_E$ and quasars spectrum for $L = 0.34L_E, 0.59L_E$ (see Appendix).

3.1 IR/optical/UV continuum

We calculate the accretion disk spectra taking into account the direct irradiation by the central source as well as the irradiation by the flux scattered in the corona, as described in Sect. 2.2. Figure 1 illustrates our results in $\log \nu f_\nu - \log \nu$ form.

In the case of low L/L_{Edd} ratio, the corona is never strong and the direct irradiation dominates, independently from the corona temperature. Therefore the adopted location of the irradiating source is of significant importance. No corona influence is seen when the temperature is lower, some redistribution of the flux towards the outer part of the disk is present when the temperature is higher.

In the case of high L/L_{Edd} ratio, the effect of the corona is essential and direct irradiation negligible which means that the location of the central source is not essential any longer (unless H_X would be very high indeed). The effect of irradiation is significant even for lower corona temperature and it is particularly strong for high temperature, leading to significant enhancement of spectra in IR/optical band.

In order to compare the derived spectra and observed continuum shapes of accretion disc we calculate the spectral indices α ($f_\nu \sim \nu^\alpha$) in optical range ($\nu \sim 10^{14.5} \div 10^{15}$ Hz) and in the following pieces of UV range $\nu \sim 10^{15.12} \div 10^{15.32}$ Hz (UV-1) and $\nu \sim 10^{15.22} \div 10^{15.36}$ Hz (UV-2). They are presented in Table 2. The mean values of spectral index for these three ranges obtained from observations by various groups for various samples of quasars we show in Table 3. It could be supplemented by the UV slope (between 15.13 and 15.45) of the composite radio quiet quasar spectrum given by Zheng et. al (1996) equal -0.86, but their formal error does not reflect the dispersion of the contributing spectra. Unfortunately, equally reliable data for Seyfert galaxies are not available since in the case of weaker active galactic nuclei the determination of the spectral slope is complicated by strong contamination of the spectra by circumnuclear starlight.

Comparing directly the predicted spectral slopes of the

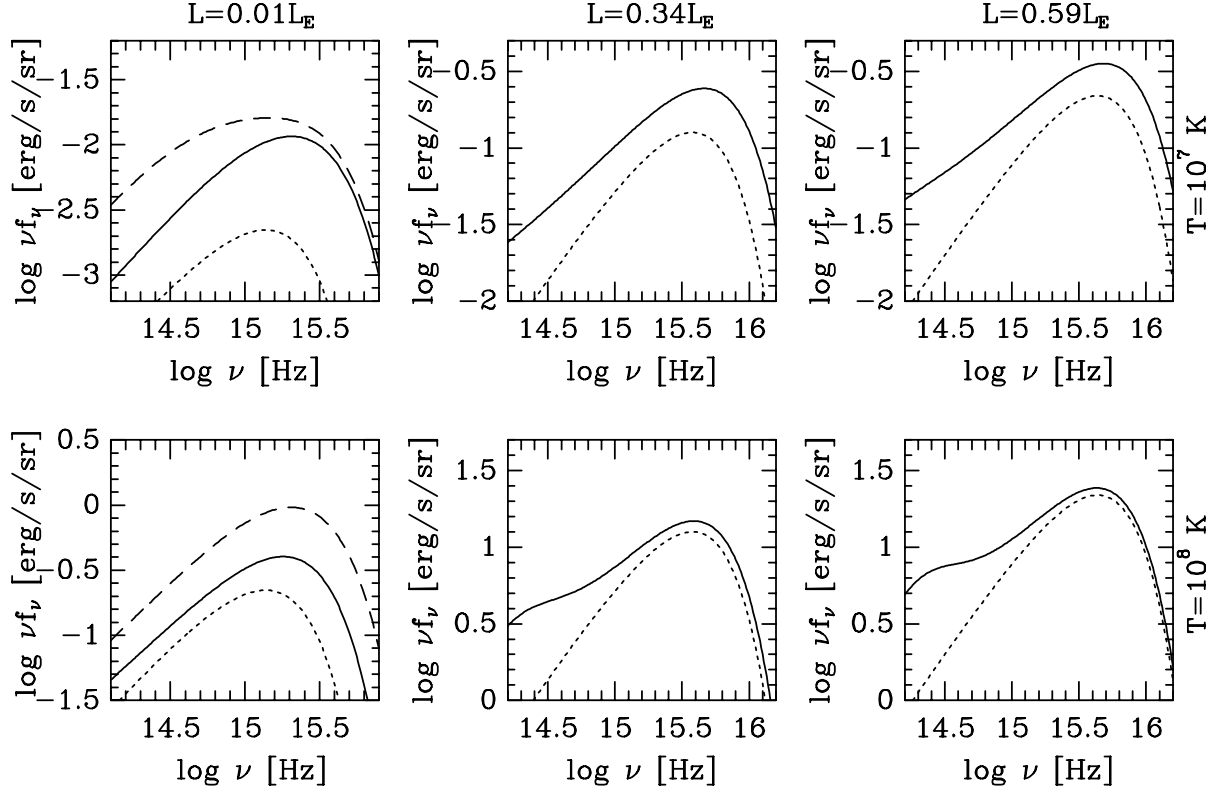


Figure 1. The spectra of irradiated accretion disks parametrized by the L/L_{Edd} ratio and the corona temperature. The dotted curves show the spectra of non-irradiated disks and the dashed ones illustrate the cases with $H_X = 33.2r_g$.

Table 2. Spectral indices in the selected ranges of continuum.

Model	α_{opt}	α_{UV-1}	α_{UV-2}
$L = 0.01L_E; T = 10^7 K;$ $H_X = 33.2r_g$	-0.5	-1.1	-1.22
$L = 0.01L_E; T = 10^7 K;$ $H_X = 3.32r_g$	0.01	-0.74	-0.94
$L = 0.01L_E; T = 10^8 K;$ $H_X = 33.2r_g$	-0.06	-0.75	-0.94
$L = 0.01L_E; T = 10^8 K;$ $H_X = 3.32r_g$	-0.1	-0.9	-1.14
$L = 0.34L_E; T = 10^7 K$	-0.19	-0.27	-0.32
$L = 0.34L_E; T = 10^8 K$	-0.55	-0.36	-0.4
$L = 0.59L_E; T = 10^7 K$	-0.32	-0.3	-0.34
$L = 0.59L_E; T = 10^8 K$	-0.66	-0.32	-0.35

high luminosity models (roughly adjusted to quasar luminosities) with the observed values we conclude that they roughly correspond to the data, taking into account large errors. However, the agreement with mean values is far from perfect since the UV slopes are too flat. This is clearly caused by adopting the value of the black hole mass equal $10^8 M_\odot$, actually too low by a factor 3 to 10. Higher values of the

Table 3. The mean values with standard deviations of spectral index obtained from observations.

α_{opt}	α_{UV-1}	α_{UV-2}
Neugebauer et al. 1987	Baldwin et al. 1989	Francis et al. 1992
-0.4 ± 0.4	-0.91 ± 0.34	-0.67 ± 0.5

in Neugebauer et al. paper the emission in 'small blue bump' is subtracted.

mass would give flatter optical spectra and steeper UV spectra due to the decrease of the disk temperature for given L/L_{Edd} ratio. It might therefore slightly favor the models with higher corona temperature. Unfortunately, the available corona models are only for $10^8 M_\odot$ (see Sect. 2.1) so we cannot support this conclusion quantitatively.

3.2 Emission lines

We can easily see that the emission of the broad emission lines by clouds formed close to the basis of the hot accretion disk corona is a reasonable assumption. The typical widths of lines reaching $FWHM \approx 2000 - 10000$ km/s correspond to Keplerian velocities over the radii range $1.3 \cdot 10^{16} cm < r < 3.4 \cdot 10^{17} cm$ in the case of an accretion

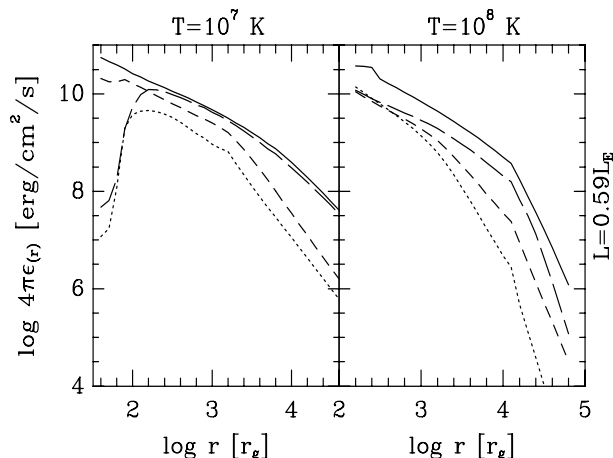


Figure 2. The examples of the radial distribution of the local line emissivity of four strongest lines as defined in Sect. 2.3.2 for $L/L_{Edd} = 0.59$ and the corona temperature 10^7 K (left panel) and 10^8 K (right panel). The solid, long-dashed, short-dashed and dotted curves represent $Ly\alpha$, CIV, HeII and NV lines respectively.

disc around $10^8 M_\odot$ black hole. It is the region covered by the corona and the cloud emissivity is large in this range (see Fig. 2). Also the line ratios should be reasonable as the cloud formation is based on special requirements as for the ionization parameter.

Detailed predictions of the model can support this scenario and allow to put some constraints on the L/L_{Edd} ratio, corona temperature and the radial distribution of clouds.

3.2.1 Line profiles

We present the calculated profiles for C_{IV} and $Ly\alpha$ lines only, because these lines are statistical investigated best of all.

Line profiles determined by the model depend on the disk/corona model and on the adopted radial distribution of the number of clouds, reflecting various assumption about their formation and destruction.

An example of the radial distribution of the local emissivity of several lines is shown in Fig. 2. It is further combined with the radial distribution of the number of clouds. In the case of model (b) (see Table 1) this distribution is preserved whilst in other models it includes additional local weight and either outer or inner parts of the distribution are enhanced.

We calculate the profiles for four values of the inclination angle of accretion disc: 0° , 30° , 60° and 80° . According to the unified scheme of AGN supported by a number of strong observational data (e.g. Antonucci 1993) objects viewed at large inclination angles are obscured by molecular/dusty torus and are not identified as quasars so the mean inclination angle is expected to be smaller than 60° .

We compare the profiles with the mean values and observed ranges of the these two line widths.

The first sample are exceptionally well studied line pro-

files of quasars by Brotherton et al. (1994). These authors analysed two quasar samples (a small sample with high quality UV spectra and the other from Large Bright Quasar Survey; hereafter ALS and LBQS) and were able to decompose the contribution to broad lines from Intermediate Line Region (distant and most probably spherical) and Very Broad Line Region. Here we use the ALS data.

The second sample (Bright Quasar Sample, BQS) is from Baldwin et al. (1989) and the third one quasars from Wills et al. (1993) which are not decomposed into ILR and VBLR, as above. In our model we expect the contribution from broad range of radii and such a decomposition might not be necessary.

In Table 4 we give the observational constraints and the results from our most promising models, i.e. case (a), (b) and (f).

Radial cloud distribution (c) gives unreasonably broad profiles for both lines since they enhance too much the emission from inner radii (the number of clouds decreases with radius far too fast). Models from families (d) and (e) gives exactly the opposite trend, leading to unreasonably narrow profiles.

Model (b) also gives too narrow profiles, although not as narrow as case (c). Slight decrease of the cloud number with radius is clearly favored.

Second and third among the class (a) models well represent the CIV distribution and require the dusty torus to cover inclination angles above $\sim 60^\circ$. However, these solutions do not satisfy the observational requirement that the $Ly\alpha$ is broader than the CIV.

We conclude that the most favorable representation is given by model (f), $L/L_{Edd} = 0.59$ and the corona temperature 10^8 K, with the torus shielding the view above $\sim 60 - 70^\circ$. This last quantity is very sensitive to the corona temperature. We find the solution with low temperature equally satisfactory if the opening angle of the torus is as small as 30° .

3.2.2 Line intensities

We compute line ratios for three models of the radial cloud distribution which were most promising from the point of view of $Ly\alpha$ and CIV profiles varying also other model parameters. The results are presented in Table 5.

We compare them with the line ratios for quasars determined by Brotherton et al. (1994) for ALS and LBQS samples, Baldwin et al. (1989), Francis et al. (1991) and Zheng et al. (1996).

The $Ly\alpha$ to CIV ratio predicted by models with the luminosity close to the Eddington luminosity and the mean quasar spectrum fall reasonably close to the observed values, although many models with low corona temperature tend to underproduce this ratio whilst high temperature corona models sometimes overproduce it.

The dispersion between different observational results is considerable but we see that low corona temperature, consistent with the inverse Compton temperature of the quasar spectra, is allowed only in case (f) and L/L_{Edd} ratio equal 0.34; all other models require higher temperature to produce the required amount of $Ly\alpha$.

Model (f), favored by the study of the line profiles, with the corona temperature somewhat below 10^8 K seems quite

Table 4. FWHMs in km/s of Ly_α and CIV lines profiles

Model	$i = 0^\circ$		$i = 30^\circ$		$i = 60^\circ$		$i = 80^\circ$	
	Ly_α	CIV	Ly_α	CIV	Ly_α	CIV	Ly_α	CIV
Model a								
$L = 0.34L_E; T = 10^7 K$	3130	3240	7070	7590	10940	12080	12450	13080
$L = 0.34L_E; T = 10^8 K$	2840	2760	5890	6700	9020	10800	9950	12150
$L = 0.59L_E; T = 10^7 K$	2980	2690	5750	5750	8880	9060	9760	10300
$L = 0.59L_E; T = 10^8 K$	2690	2690	5194	4900	7710	7400	8440	8070
Model b								
$L = 0.01L_E; T = 10^8 K; H_X = 33.2r_g$	2700	2700	3980	4090	5670	5780	6220	6340
$L = 0.01L_E; T = 10^8 K; H_X = 3.32r_g$	2800	2800	4460	4720	6670	7040	7150	7900
$L = 0.34L_E; T = 10^7 K$	2620	2610	3430	3390	4680	4670	5200	5270
$L = 0.34L_E; T = 10^8 K$	2620	2650	3510	3790	5450	5670	6010	6340
$L = 0.59L_E; T = 10^7 K$	2620	2690	3200	3280	4346	4462	5000	5100
$L = 0.59L_E; T = 10^8 K$	2600	2610	3790	3790	5670	5780	6300	6450
Model f								
$L = 0.34L_E; T = 10^7 K$	5120	2910	16690	11860	> 20000	~ 20000
$L = 0.34L_E; T = 10^8 K$	2870	2870	9320	9770	15360	16020	17240	17970
$L = 0.59L_E; T = 10^7 K$	4050	2840	11050	9360	16830	15210	19200	16700
$L = 0.59L_E; T = 10^8 K$	2730	2730	6810	6260	10610	9500	11790	10550
Observations								
Brotherton et al. (1994)ALS	Ly_α : 8000 ± 600				CIV: 6800 ± 300			
Baldwin et al. (1989)BQS	CIV: $2500 \div 8000$; mean= 5680 ± 390							
Wills et al. (1993)	CIV: $1970 \div 10400$; mean= 4870 ± 180							

attractive if compared, for example, with Zheng et al. (1996). It could reproduce well the Ly_α to CIV ratio as well as the amount of NV and (perhaps) SiIV. However, it overproduces HeII line, although this discrepancy is not so strong if other samples are considered. It also underproduce some other weak lines like AlIII, SiIII] and CIII].

However, it is possible that there is a contribution to the line emission from collisional excitation. In the case of clouds moving across the corona it is only natural to expect the formation of the shock at the cloud front and therefore some additional ionization. This effect was neglected in our study.

4 CONCLUSIONS

Presented results support the following view of quasars.

Quasars are radiating at L/L_{Edd} ratio ~ 0.5 , accretion disk in these objects is surrounded by a hot corona with temperature higher than the inverse Compton temperature. Broad emission lines observed in their spectra come from clouds which form continuously at the basis of the corona due to thermal instabilities and are being blown out by the radiation pressure until they are destroyed when they reach supersonic velocities, $\sim 2000\text{km/s}$.

However, further studies are necessary to confirm this picture. For example, extension of the computations towards higher values of the mass of the black hole and the inclusion

of the contribution from collisionally heated sides of moving clouds may be essential.

ACKNOWLEDGEMENTS

We thank Gary Ferland for providing us with his photoionization code CLOUDY version 80.07. We are grateful to Agata Różańska for many helpful discussions. This work was supported in part by grants 2P03D00410 and 2P30D02008 of the Polish State Committee for Scientific Research.

APPENDIX

We parametrize the continua emitted by the central regions of the accretion flow by adopting fixed values of the energy index α in a number of energy bands given in $\log\nu$. In the case of Seyfert galaxies we assume 10.5 - 14.83 ($\alpha = 2.5$), 14.83 - 15.76 (-0.5), 15.76 - 16.12 (-1), 16.12 - 16.60 (-3), 16.60 - 18.70 (-0.7), 18.70 - 19.37 (-0.9), 19.37 - 22.37 (-1.67). In the case of quasars we assume 10.5 - 14.83 ($\alpha = 2.5$), 14.83 - 15.76 (-0.5), 15.76 - 16.12 (-1), 16.12 - 17.05 (-3), 17.05 - 19.37 (-0.7), 19.37 - 22.37 (-1.67).

Table 5. Line Intensity Ratios

Model	$Ly\alpha$ 1216	NV 1240	CII 1335	SiIV 1397	OIV] 1402	CIV 1549	HeII 1640	OIII] 1663	AlIII 1859	SiIII] 1892	CIII] 1909
Model a											
$L = 0.01L_E; T = 10^8 K; H_X = 33.2r_g$	80	19	0	16	8	100	18	4	2	2	3
$L = 0.01L_E; T = 10^8 K; H_X = 3.32r_g$	92	23	0	10	10	100	15	5	1	2	5
$L = 0.34L_E; T = 10^7 K$	114	15	0	0	4	100	76	0	0	0	0
$L = 0.34L_E; T = 10^8 K$	239	33	0	19	8	100	45	3	1	3	3
$L = 0.59L_E; T = 10^7 K$	144	20	0	1	1	100	58	2	0	0	1
$L = 0.59L_E; T = 10^8 K$	239	25	0	19	7	100	42	2	1	3	2
Model b											
$L = 0.01L_E; T = 10^8 K; H_X = 33.2r_g$	83	4	0	7	3	100	6	7	1	3	14
$L = 0.01L_E; T = 10^8 K; H_X = 3.32r_g$	84	6	0	6	4	100	6	7	1	2	14
$L = 0.34L_E; T = 10^7 K$	132	5	0	1	2	100	24	1	0	0	0
$L = 0.34L_E; T = 10^8 K$	276	8	1	14	5	100	21	8	1	10	14
$L = 0.59L_E; T = 10^7 K$	125	6	0	1	3	100	12	2	0	0	1
$L = 0.59L_E; T = 10^8 K$	226	7	0	13	4	100	20	3	1	8	5
Model f											
$L = 0.34L_E; T = 10^7 K$	210	34	0	0	3	100	144	0	0	0	0
$L = 0.34L_E; T = 10^8 K$	234	46	0	21	9	100	55	1	2	2	1
$L = 0.59L_E; T = 10^7 K$	166	25	0	1	1	100	83	1	0	0	0
$L = 0.59L_E; T = 10^8 K$	250	37	0	22	9	100	54	2	2	2	1
Observations											
Brotherton et al. (1994)ALS	219	111	6		42	100	31	0	17	<5	41
Brotherton et al. (1994)LBQS	154	137	6		55	100	40	0	22	...	59
Baldwin et al. (1989)BQS	236	106	100	30		16	...	43
Francis et al. (1991)LBQS	159		4		30	100	29		46(AlIII + CIII)		
Zheng et al. (1996)	192	27	1		16	100	7	5	6	5	23

REFERENCES

- Antonucci R., 1993, *Ann. Rev. A&A*, 31, 473
 Baldwin J.A., Wampler W.J., Gaskell C.M., 1989, *ApJ*, 338, 630
 Begelman M.C., McKee C.F., Shields G.A., 1983, *ApJ*, 271, 70
 Begelman M.C., McKee C.F., 1983, *ApJ*, 271, 89
 Brotherton M.S., Beverley J.W., Francis P.J., Steidel C.C., 1994, *ApJ*, 430, 495
 Chen K., Halpern J.P., 1989, *ApJ*, 344, 115
 Czerny B., Elvis M., 1987, *ApJ*, 321, 305
 Czerny B., Lehto H.J., 1996, in preparation
 Fabian A.C., Guilbert P.W., 1982, *MNRAS*, 199, 1045
 Fabian A.C., Guilbert P.W., Arnaud K., Shafer R.R., Tennant A., Word M., 1986, *MNRAS*, 218, 457
 Fabian A.C. et al., 1994, *PASJ*, 46, L59
 Francis P.J., Hewett P.C., Foltz C.B., Chaffee F.H., 1992, *ApJ*, 398, 476
 Greenhill L.J., Jiang D.R., Moran J.M., Reid M.J., Lo U.Y., Claussen M.J., 1995, *ApJ*, 440, 619
 Haardt F., Maraschi L., Ghisellini G., 1994, *ApJ*, 432, L95
 Harms R.J., Ford H.C., Tsvetanov Z.I., Hartig G.F., Dressel L.L., Kriss G.A., Bohlin R., Davidsen A.F., Margon B., Kochnar A.K., 1994, *ApJ*, 435, L35
 Henri, G. & Pelletier, G., 1991, *ApJ Letters*, 383, L7
 Hure J.M., Collin-Soufrin S., Le Bourlot J., Pineau Des Forets G., 1994, *A&A*, 290, 19
 Krolik J.H., McKee C.F., Tarter C.B., 1981, *ApJ*, 249, 422 [KMT]
 Mathews W.G., Ferland G.J., 1987, *ApJ*, 323, 456
 Matsuoka M., Yamauchi M., Piro L., Murakami T., 1990, *ApJ*, 361, 440
 McClintock J.E., London R.A., Bond H.E., Albert, D.G., 1982, *ApJ*, 258, 245
 McKee C.F., Begelman M.C., 1990, *ApJ*, 358, 392
 Murray S.D., Castor J.I., Klein L.I., McKee C.F., 1994, *ApJ*, 435, 631 [MCKM]
 Mushotzky R.F., Done C., Pounds K.A., 1993, *Ann. Rev. A&A*, 31, 440
 Neugebauer G., Green R.F., Matthews K., Schmidt M., Soifer B.T., Bennett J., 1987, *ApJS*, 63, 615
 Ostriker E.C., McKee C.F., Klein, R.I., 1991, *ApJ*, 377, 593 [OMK]
 Page D.N., Thorne K.S., 1974, *ApJ*, 191, 499
 Pounds K.A., Nandra K., Stewart G.C., George I.M., Fabian, A.C., 1990, *Nature*, 344, 132
 Raymond J.C., 1993, *ApJ*, 412, 267
 Rees M.J., 1984, in *Max-Planck Inst. für Physik und Astrophysik X-Ray and UV Emission from Active Galactic Nuclei*, p.138
 Ross R.R., Fabian A.C., 1993, *MNRAS*, 261, 74
 Różańska, A., Czerny, B., 1996, *Acta Astron.*, 46, 233
 Shakura N.I., Sunyaev, R.A., 1973, *A&AS*, 24, 337
 Shimura T., Takahara F., 1995, *ApJ*, 440, 610
 Siemiginowska A., Czerny B., Kostyunin, V., 1996, *ApJ*, 458, 491
 Spitzer L., 1978, *Physical Processes in the Interstellar Medium*, New York, Wiley
 Stern B.E., Poutanen J., Svensson R., Sikora M., Begelman M.C.,

- 1995, ApJ, 449, 13
Walter R., Fink H.H., 1993, A&A, 274, 105
White N.E., Holt S.S., 1982, ApJ, 257, 318
Wilkes B.J., Elvis M., 1987, ApJ, 323, 243
Williams O.R. et al., 1992, ApJ, 389, 157
Wills B.J., Brotherton M.S., Fong D., Steidel C.C., Sargent W.L.,
1993, ApJ, 415, 563
Yaqoob, T., 1990, PhD Thesis, University of Leicester
Życki P.T., Czerny, B., 1994, MNRAS, 266, 653
Życki P.T., Krolik J.H., Zdziarski A.A., Kallman T., 1994, ApJ,
437, 597

This paper has been processed by the authors using the
Blackwell Scientific Publications L^AT_EX style file.